Immobilization of Ag nanoparticles/FGF-2 on a modified titanium implant surface and improved human gingival fibroblasts behavior

Qianli Ma,[1] Shenglin Mei,[1] Kun Ji,[1] Yumei Zhang,[1] Paul K. Chu[2]

[1]School of Stomatology, The Fourth Military Medical University, 17 West Chang Le Road, Xi'an 710032, China
[2]Department of Physics and Materials Science, City University of Hong Kong, Tat Chee Avenue, Kowloon, Hong Kong, China

Received 25 October 2010; revised 27 February 2011; accepted 10 March 2011
Published online 27 May 2011 in Wiley Online Library (wileyonlinelibrary.com). DOI: 10.1002/jbm.a.33111

Abstract: The objective of this study was to form a rapid and firm soft tissue sealing around dental implants that resists bacterial invasion. We present a novel approach to modify Ti surface by immobilizing Ag nanoparticles/FGF-2 compound bioactive factors onto a titania nanotubular surface. The titanium samples were anodized to form vertically organized TiO_2 nanotube arrays and Ag nanoparticles were electrodeposited onto the nanotubular surface, on which FGF-2 was immobilized with repeated lyophilization. A uniform distribution of Ag nanoparticles/FGF-2 was observed on the TiO_2 nanotubular surface. The L929 cell line was used for cytotoxicity assessment. Human gingival fibroblasts (HGFs) were cultured on the modified surface for cytocompatibility determination. The Ag/FGF-2 immobilized samples displayed excellent cytocompatibility, negligible cytotoxicity, and enhanced HGF functions such as cell attachment, proliferation, and ECM-related gene expression. The Ag nanoparticles also exhibit some bioactivity. In conclusion, this modified TiO_2 nanotubular surface has a large potential for use in dental implant abutment. © 2011 Wiley Periodicals, Inc. J Biomed Mater Res Part A: 98A: 274–286, 2011.

Key Words: dental implants, TiO_2 nanotubes, FGF-2, silver nanoparticles, real-time PCR

INTRODUCTION

Dental implants are widely used to treat edentulous,[1–3] however failure may occur due to peri-implantitis. Tight and healthy implant-connective tissue integration, which is the most essential part of the peri-implant soft tissue (PIST) seal, forms a foundation to prevent epithelial downgrowth[4] and protects the bone tissue beneath from bacterial and mechanical damage. Tissue healing around the implant can be influenced by the shape, design, physicochemical property, and microtopography of the implant surface[5]. Polished Ti and Ti alloys are conventionally used in the trans-gingival part of dental implant abutment, but they are unable to form a tight PIST seal or prevent bacterial invasion. Anodization can form a titania nanotubular surface[6] with a relatively large surface area. This properties of this surface facilitate immobilization of antibacterial agents[7] and growth factors[8] on the surface of the implant. The cell response depends on the nanoscale surface features of the TiO_2 nanotube array. The microtopography of TiO_2 nanotube array can affect cell adhesion, orientation, proliferation, gene expression, and signaling.[9–11] Cell types such as osteoblasts, fibroblasts, mesenchymal stem cells, epithelia, and so on, adhere and proliferate best on nanotubes ranging in size from 30 to 120 nm.[8,12–17] It has been reported that HGFs adhere, survive, and proliferate better on TiO_2 nanotube arrays with a tube diameter of ~120 nm and better electrochemical stability in artificial saliva has also been observed.[18]

Ag-deposited TiO_2 nanotubular surfaces show lower toxicity and higher osteoblast proliferation than polished Ti.[19] Silver possesses the highest antimicrobial properties among metals[20,21] and has potential bioactivity. The physicochemical properties are considered essential factors in the antimicrobial activity of Ag. There has been a great deal of interest in the use of Ag nanoparticles to prevent or control periimplant infection because Ag nanoparticles are considered to be less toxic than Ag^+ but have the same or higher antimicrobial properties. In general, particles less than 10 nm are more toxic to bacteria such as *Escherichia coli* and *Pseudomonas aeruginosa*.[22,23] In addition, as a wound healing-accelerator, growth factors are known to affect cell proliferation, differentiation, and other functions. The fibroblast growth factors (FGFs) comprise a large family of polypeptide growth factors.[24] FGFs exert their proangiogenic activity and induce chemotaxis in endothelial cells by interacting with various endothelial cell surface receptors[25] including tyrosine kinase receptors, heparin-sulfate proteoglycans, and integrins.[26] FGFs may also induce the production of various ECM components[27] and contribute to the maturation of new vessels. It has been shown that fibroblast growth factor 2 (FGF-2) is a potent mitogen in a variety of cells including fibroblasts, mesenchymal cells, and osteoblasts, and is

Correspondence to: Y. Zhang; e-mail: wqtzym@fmmu.edu.cn or P. K. Chu; e-mail: paul.chu@cityu.edu.hk
Contract grant sponsor: The National Natural Science; contract grant number: 81070862.
Contract grant sponsor: City University of Hong Kong Strategic Research; contract grant number: 7008009.
Contract grant sponsor: Hong Kong Research Grants Council (RGC) General Research Funds (GRF); contract grant number: CityU 112510

effective in regulating the proliferation and ECM gene expression of fibroblasts.[28,29] Moreover, FGF-2 can be easily immobilized on oxygen plasma treated titanium.[30] Cell adhesion and proliferation on various surface topographies have been investigated.[31–33] However, adhesion and proliferation of Human Gingival Fibroblasts (HGFs) around the dental implant need to be studied more extensively to mimic integration between dental implant abutment and surrounding soft tissues. Moreover, the cytocompatibility and interactions between HGFs and Ag nanoparticles have not been investigated systematically.

In the work reported here, titanium is anodized at 20 V to produce a vertical and highly organized TiO_2 nanotube array. Silver nanoparticles, which could indeed improve the bioactivity and antimicrobial characteristics,[19] are electrodeposited on the nanotubular surface. FGF-2 is immobilized on the Ag-loaded TiO_2 nanotubular surface by successive lyophilization. The aim of this study is to create a modified Ti surface with lower cytotoxicity and antibacterial properties and investigate the behavior of HGFs cultured on the nanotubular surface with Ag nanoparticles/FGF-2.

MATERIALS AND METHODS

Sample preparation

Preparation of PT(Polished Ti) and NT(NanoTube) samples. Pure Ti (Titanium) foils (99.9%, 1000 × 500 × 0.6 mm^3) were cut into 10 × 10 × 0.6 mm^3 samples, polished with 400–1500 grits SiC sandpapers, ultrasonically cleaned in acetone, 70% ethanol, and double distilled water (DDW) for 10 min in sequence, and then dried in N_2 at 50°C for 20 min. The PT samples were anodized in an electrolyte containing 0.5% NH_4F and 1 mol/L $(NH_4)_2SO_4$ at 20 V for 45 min with Ti anode and Pt cathode under constant stirring. After the reaction, anodized samples were ultrasonically cleaned and dried to obtain the NT (nanotubular) samples.

Preparation of NT-Ag(Ag-loaded NanoTube) and NT-Ag-F(Ag/FGF-2-immobilized NanoTube) samples. To immobilize Ag onto the TiO_2 nanotubular surface, a Pt anode and a NT cathode were used for Ag electrodeposition, in a 0.003 mol/L $AgNO_3$ electrolyte by applying 2V with a 100 mA current for 30 seconds using constant stirring. Afterwards, Ag particles were electrodeposited onto the TiO_2 nanotubular surface. These samples were ultrasonically cleaned, as described above, to remove unconjugated Ag particles and dried in N_2. These samples were sterilized by ultraviolent A/C(UVA/C) irradiation for 2 h because UV-A activated the photocatalytic property of TiO_2 to remove organic contamination and inactive bacteria. The E. coli source recombinant human FGF-2 (Peprotech, UK) was reconstituted in a Tris-HCl buffered solution (pH = 7.6) with 0.1% bovine serum albumin (BSA). The FGF-2 solution was diluted to 500 ng/mL. NT-Ag samples were incubated in this FGF-2 solution for 10 min at 4°C and then lyophilized. This procedure was repeated three times and these samples were stored under sterile conditions.

Surface analysis

Surface characterization. Surface and material characterization studies were conducted on four types of samples designated as PT, NT, NT-Ag, and NT-Ag-F. The surface chemical analysis was performed using X-ray photoelectron spectroscopy (XPS, Al K_α, 1486.6 eV Axis Ultra, Kratos, UK). The X-ray generated Auger electron spectrum, was analyzed to identify the chemical state of Ag. Field emission scanning electron microscopy (FE-SEM, JSM-6460, JEOL, Japan) and atomic force microscopy (AFM, SPM400, SEIKO, Japan) were employed to analyze the surface topography and roughness of samples. The surface contact angles were measured by analyzing the drop shape of DDW and diiodomethane using a contact angle measuring system (KRUSS, Germany) and the surface free energy was calculated by Owens equation.[34]

Morphological observation of immobilized FGF-2. The FGF-2 on NT-Ag-F samples was examined by an immunofluorescence assay. After FGF-2 immobilization, the samples were washed three times with phosphate-buffered saline (PBS, pH = 7.4) for 5 min, treated with rabbit anti-bFGF polyclonal antibody (1:200; Sigma) as the primary antibody at 4°C overnight, and washed three times with PBS. The samples were then treated with FITC-label goat antirabbit IgG (1:200; BOIS, China) for 1 h at 37°C and washed thrice in PBS (pH = 7.4). The samples were inspected by scanning laser confocal microscopy (Olympus FV-1000, Japan). To evaluate the remaining FGF-2 on the nanotubular surface after a longer period, a part of the NT-Ag-F sample was incubated in PBS at 37°C for 9 days and the immunofluorescence procedures as described above were repeated.

Determination of cytotoxicity

This assay was conducted in accordance with ISO 10993-5.[35] Aluminum oxide ceramic rods/phenol were used as the negative/positive controls, respectively. Samples were incubated in DMEM at 50°C for 72 h to form extracts. The L929 cells (CELL BANK, Japan) were cultured in Dulbecco's minimum essential medium (pH = 7.4, DMEM, Gibco) with 5% bovine calf serum (BCS. Gibco) and 1% penicillin/gentamicin, and incubated in a humidified atmosphere of 5% CO_2 at 37°C. L929 cells were seeded onto a 96-well dish (~1000 cells/well) and maintained for 24 h to form a semi-confluent monolayer.[36] After removing the culture medium, cells were exposed to 100 μL of extracts at 100% and 100 μL of DMEM without any extract was added to the blank well. After 24, 48, and 72 h, the culture medium was discarded and 50 μL of the 3-(4,5-dimethylthiazol-2-yl)-2,5-diphenyl tetrazolium bromide (MTT) solution (1 mg/mL) was added to each well and incubated for 2 h at 37°C under 5% CO_2. The MTT solution was removed and 100 μL of dimethyl sulfoxide (DMSO, Sigma) was added to each well. The optical density (OD) value at 570 nm (650 nm reference) was determined. A drop in the cellular vitality resulted in reduced metabolic activity. This decrease was directly correlated to the amount of blue-violet formazan formed, as monitored

by the optical density at 570 nm on a spectrophotometer (Bio-tek). To calculate the reduction in the viability compared to the blank, the following equation was used:

$$\text{Relative Growth Rate (RGR, \%)} = \frac{\text{OD570e}}{\text{OD570b}} \times 100\%.$$

Here, OD_{570e} is the mean value of the measured optical density of the 100% extract from the sample and OD_{570b} is the mean value of the measured optical density of the blank. The lower the RGR value, the higher the cytotoxic potential of the sample. If the RGR value is reduced to <70% of the blank, it is potentially cytotoxic.[35]

Evaluation of behavior of HGFs

Evaluation of cell attachment and proliferation. HGFs were obtained from periodontal-healthy patients (18−32 years of age) through third molar extraction. The gingival tissue was washed twice in PBS containing 10,0000 U penicillin/gentamecin and incubated in a dispase solution (Gibco) overnight to separate connective tissues from the epithelium. The gingival tissues were then sheared into 1.0 × 1.0 × 1.0 mm^3 blocks, which were cultured in DMEM with 10% fetal calf serum (FCS Gibco) and 100,000 u penicillin/gentamecin and incubated in a humidified atmosphere of 5% CO_2 at 37°C. Passage 4 HGFs were used for further analysis. HGFs were then seeded on the samples (serum-free) of each group at a concentration of 1×10^5 cells/mL ($\sim 5 \times 10^4$ cells/cm^2) and the culture was incubated for 30, 60, and 120 min to allow adhesion. At each time point, samples were washed with PBS to remove non-attached cells. Four percent of formalin solution was used to fix the cells, which were stained with 4′,6′-diamidino-2-phenylindole (DAPI, Roche) at a concentration of 1 μg/mL. The images were then captured from three random fields (2.60 × 1.94 mm^2) by a fluorescence microscope (Leica DMI6000B, Germany). The cell adhesion number was counted by the Image J software and the results were presented as relative cell adhesion rates (RCAR) as follows:

$$\text{RCAR}(\%) = \frac{\text{COUNTS}}{\text{COUNTP}} \times 100\%$$

Here, COUNTs represents the mean value of the count number on the samples and COUNTp is the mean value of the count number on the polished Ti control.

Cell proliferation was evaluated by the MTT assay. Briefly, four types of samples (each type was conducted in triplicate) were set in a 24-well dish and 4×10^4 HGF cells were seeded in each well and cultured in DMEM with 10% BCS. At days 3, 6, and 9, samples were gently washed three times with PBS and placed into a new 24-well dish. The MTT-PBS (Amresco) solutions (5 mg/mL) were prepared and filter sterilized. Two hundred microliter of the MTT solution and 800 μL of serum-free/phenol red-free DMEM were added to each well and the samples were incubated at 37°C for 4 h to form formazen. Afterwards, formazen was dissolved in dimethyl sulfoxide (DMSO) [1 mL/well]. Two hundred microliter of this mixed solution was transferred to a new 96-well dish and the OD value of each well was monitored at 490 nm using a spectrophotometer (Bio-tek).

TABLE I. Primers Used in Quantitative PCR

Target cDNA primer sequence
Type I collagen
Forward: 5′-TCTAGACATGTTCAGCTTTGTGGAC-3′
Reverse: 5′-TCTGTACGCAGGTGATTGGTG-3′
PCR product size: 134 bp
Type III collagen
Forward: 5′-GCAAATTCACCTACACAGTTCTGGA-3′
Reverse: 5′-CTTGATCAGGACCACCAATGTCATA-3′
PCR product size: 147 bp
VEGF
Forward: 5′-GAGCCTTGCCTTGCTGCTCTAC-3′
Reverse: 5′-CACCAGGGTCTCGATTGGATG-3′
PCR product size:148 bp
Integrin β
Forward: 5′-TGTGTCAGACCTGCCTTGGTG-3′
Reverse: 5′-AGGAACATTCCTGTGTGCATGTG-3′
PCR product size: 105 bp
Fibronectin
Forward: 5′-ACCTACGGATGACTCGTGCTTTGA-3′
Reverse: 5′-CAAAGCCTAAGCACTGGCACAACA-3′
PCR product size: 116
ICAM-1
Forward: TGAGCAATGTGCAAGAAGATAGC
Reverse: CCCGTTCTGGAGTCCAGTACA
PCR product size: 105
GAPDH(house-keeping gene)
Forward: 5′-GCACCGTCAAGGCTGAGAAC-3′
Reverse: 5′-TGGTGAAGACGCCAGTGGA-3′
PCR product size: 138 bp

ECM-related gene expression. Expressions of the ECM related genes were analyzed using the real-time polymerase chain reaction (RT-PCR). The HGFs were cultured in the same manner as the proliferation assay. The total RNA of each sample was extracted with the TRIzol reagent (Gibco). One microgram total RNA of each sample was reverse transcribed into complementary DNA (cDNA, 50 μL system) using the PrimeScript™ RT reagent kit (TaKaRa, Japan). Quantitative PCR was measured on the ABI7500 Real-Time PCR System to determine the mRNA expression of the ECM-related genes including Type I/III collagen, VEGF, integrinβ, Fibronectin, and ICAM-1 using SYBR® Premix Ex™ TaqII (TaKaRa, Japan). The forward and reverse primers for the selected genes are listed in Table I. All PCR efficiencies were compared. The relative expression levels for each gene of interest were normalized to the expression of the housekeeping gene GAPDH by calculating ΔCt ($Ct_{\text{gene of interest}} - Ct_{GAPDH}$) and expression of the different genes is expressed as $2^{-(\Delta Ct)}$. The gene expression of PT as the control was normalized to 1. The specificity of every pair of PCR primers was confirmed by analyzing the melting curves. The data were analyzed using the Applied Biosystem Software using the Excel® format.

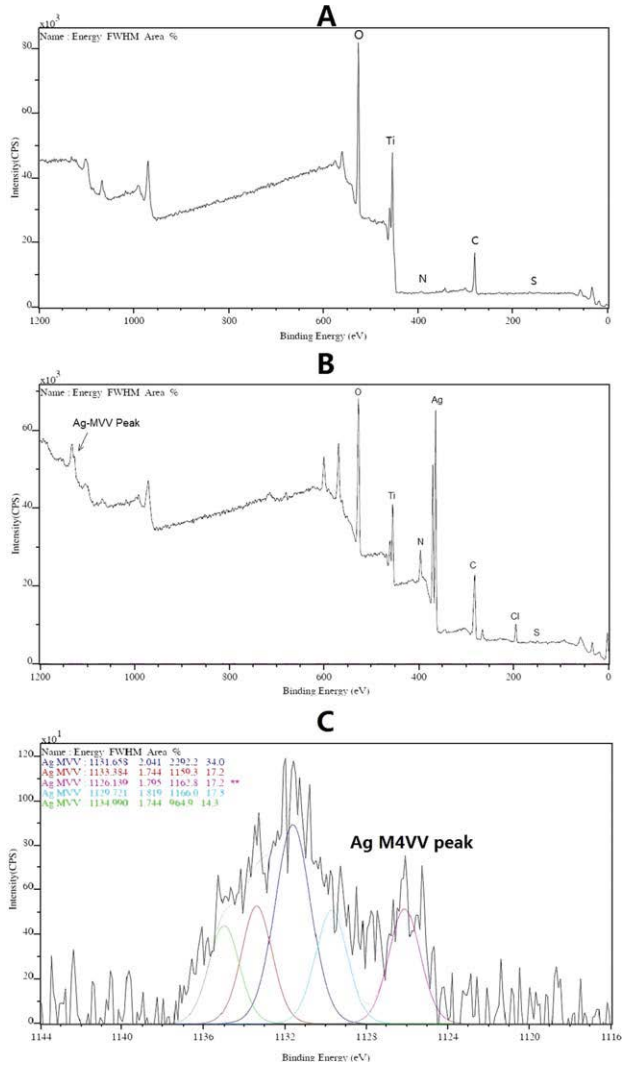

FIGURE 1. XPS analysis results: (A) NT showing only Ti and O, (B) NT-Ag showing Ti, O, and Ag, (C) X-ray induced Auger electron spectrum (XAES) of the Ag nanoparticles showing the metallic state of Ag. [Color figure can be viewed in the online issue, which is available at wileyonlinelibrary.com.]

Statistical analysis

The data were analyzed using SPSS 18.0 (SPSS). The results are expressed as means ± SD and analyzed by one-way ANOVA followed by a Student-Newman-Keuls post hoc test to assess whether there was a significant difference between the groups. When p was less than 0.01, the difference was considered significant.

RESULTS

Surface characterization

The XPS results acquired from NT/NT-Ag are displayed in Figure 1. Figure 1(A) does not show the presence of Ag but Ag is observed from NT-Ag as shown in Figure 1(B). In the X-ray induced Auger electron spectrum (XAES) [Fig. 1(C)], the Ag M_4VV peak at 1126.1 eV was detected and the Δ_c value was calculated for further correction as follows:

$$\Delta_c = C1S_{standard} - C1S_{test}$$
$$= 284.8 - 281.85 = 2.95\ \text{eV}(C1S_{standard} = 284.8\ \text{eV})$$

The Ag M_4VV kinetic energy (E_K^A) is also calculated and the Ag binding energy (E_B^P) is corrected by the following equations:

$$E_K^A = \text{AlK}\alpha\ \text{output value} - (\text{Ag}M_4\text{VV peak value} + \Delta_c)$$
$$= 1486.6 - (1126.14 + 2.95) = 357.5\text{eV}$$

$$E_B^P = \text{Ag binding energy}_{test} + \Delta_c = 368.1\ \text{eV}$$

E_B^P/E_K^A is used as the abscissa/ordinate to find out the Ag valence referenced to the XPS handbook and the Ag particles are found to be metallic.[37]

FE-SEM images of samples in Figure 2 show different microtopographies of NT and NT-Ag. The TiO_2 nanotubes formed a vertically organized array with a diameter of 100−120 nm. On the Ag-loaded nanotubular surface, most nanoparticles were 10 nm and were distributed uniformly on the TiO_2 nanotube walls. XPS results revealed that these nanoparticles were metallic Ag. The surface topographies

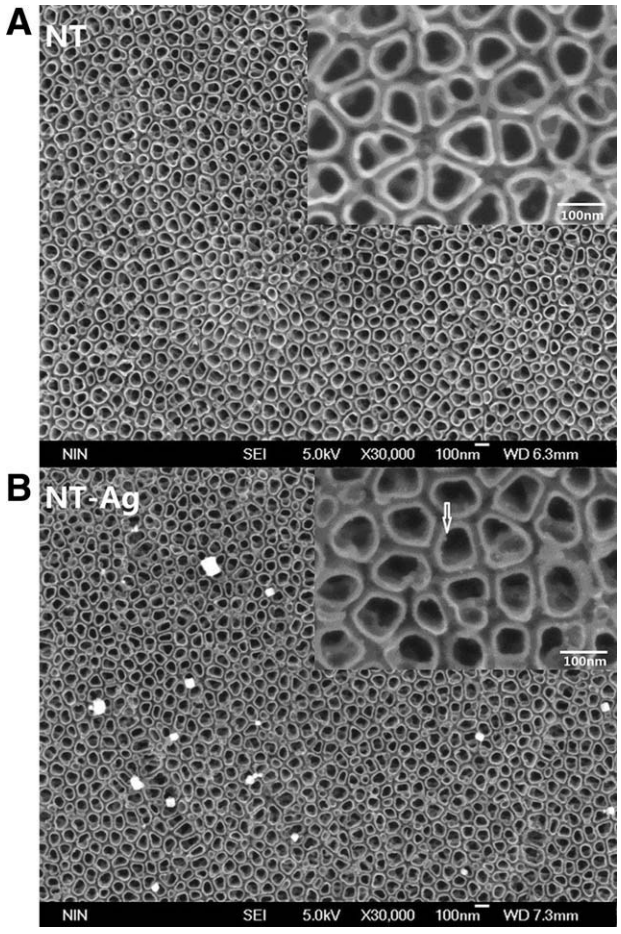

FIGURE 2. FE-SEM results: (A) NT surface shows a nanotube array structure and (B) NT-Ag surface shows adherent Ag nanoparticles uniformly distributed on the TiO_2 nanotube walls.

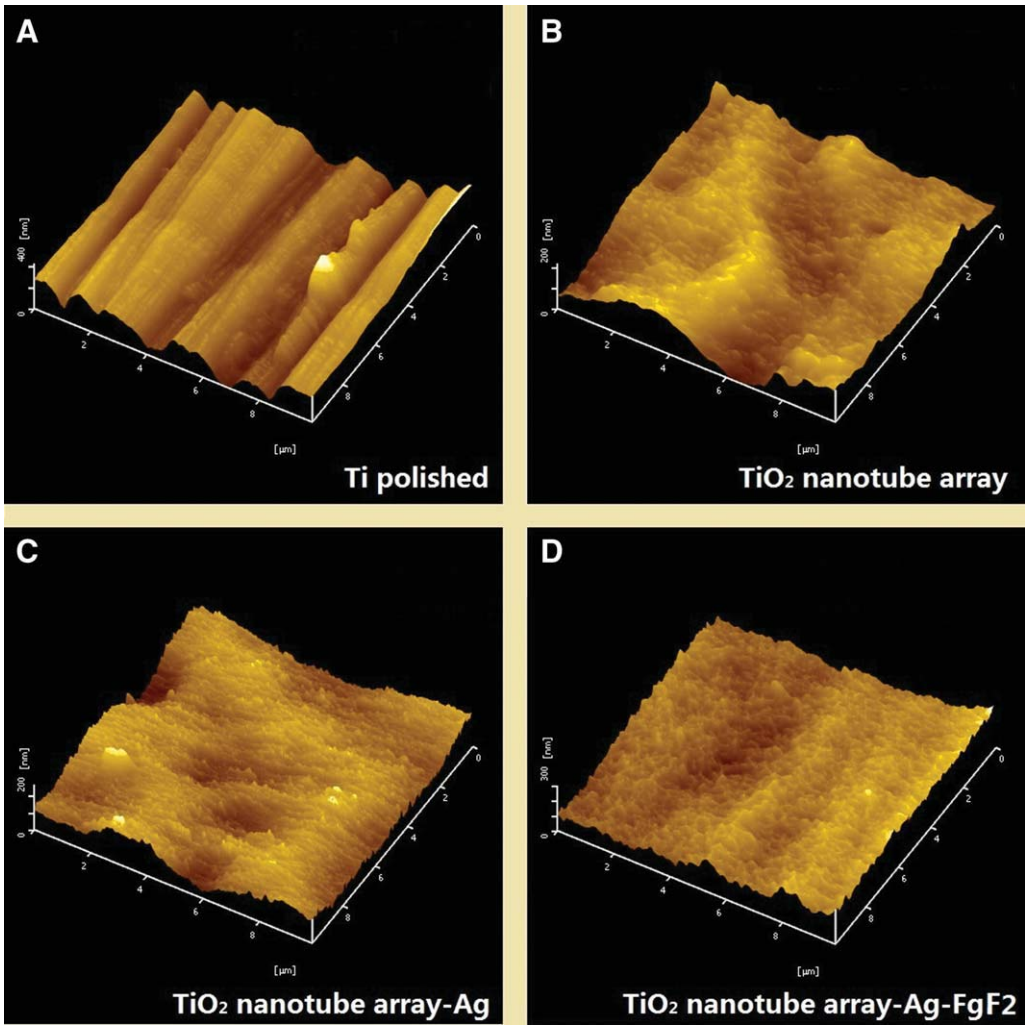

FIGURE 3. AFM images of different surfaces: (A) PT, (B) NT, (C) NT-Ag, and (D) NT-Ag-F. [Color figure can be viewed in the online issue, which is available at wileyonlinelibrary.com.]

are displayed in Figure 3. PT indicated microgroove like surface morphology, which was approximately two times rougher that of NT and NT-Ag. The NT, NT-Ag, and NT-Ag-F surfaces show a similar nanoporous structure. Interestingly, NT-Ag as slightly rougher than NT, and NT-Ag-F was rougher than NT-Ag (Table II). Anodization smoothed the surface of Ti, but Ag and FGF-2 immobilization made the surface rougher. These results also confirmed the presence of FGF-2 on NT-Ag. Figure 4 shows the contact angles and calculated surface free energies of the samples. NT and NT-Ag exhibited smaller contact angles for both DDW and diiodomethane compared to PT. However, NT-Ag-F showed a considerable increase in the contact angles for both liquids. This may be attributed to the roughness after immobilization of FGF-2 on NT-Ag-F whereas the surface free energies of NT and NT-Ag are similar but higher than those of PT and NT-Ag-F. The FGF-2 immobilized surface (NT-Ag-F) generated fluorescence both in the initial stage and after 9 days, but no fluorescence was be observed from NT-Ag (Fig. 5). These results proved that FGF-2 was indeed immobilized on the TiO_2 nanotubular surface and remains for a long time (9 days).

Cytotoxicity determination

There was no statistical difference in cellular response (Fig. 6) or RGR (Table III) observed from the MTT assay of all samples compared to the blank except the positive control at all time

TABLE II. Measurement of Surface Roughness Using AFM

	R_a	RMS	R_z (10 points)
PT	58.17 nm	71.51 nm	128.5 nm
NT	27.76 nm	34.33 nm	260.5 nm
NT-Ag	29.10 nm	35.99 nm	128.1 nm
NT-Ag-F	34.18 nm	42.06 nm	156.2 nm

R_a is the roughness average; RMS is the root mean square roughness; and R_z (10 points) is the height of irregularities of 10 points.

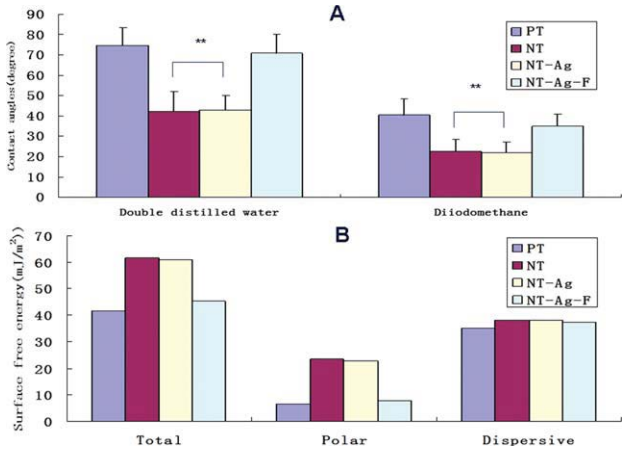

FIGURE 4. Surface free energy analysis: (A) Contact angles and (B) surface free energies. **↓($p < 0.01$). [Color figure can be viewed in the online issue, which is available at wileyonlinelibrary.com.]

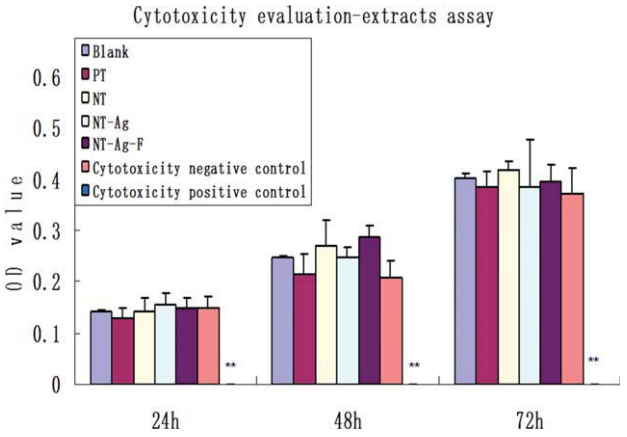

FIGURE 6. Cytotoxicity determination by extract assay. No cytotoxicity is observed except positive control. **↓($p < 0.01$). [Color figure can be viewed in the online issue, which is available at wileyonlinelibrary.com.]

points. NT-Ag showed no inhibition (RGR > 70%) of cellular vitality compared to the blank.

Behavior of HGFs

Cell adhesion values, assayed by counting the cells stained with DAPI, are displayed in Figure 7(A) at time intervals as described previously. The cell adhesion number on NT-Ag-F was larger than those on PT, NT, and NT-Ag, and this phenomenon was observed at all three time intervals. The RCARs are shown in Figure 7(B). NT and NT-Ag express low RCAR. Moreover, NT-Ag showed the lowest RCAR whereas NT-Ag-F showed the highest RCAR in this study. The pure TiO_2 nanotubular surface without immobilized FGF-2 seemed to inhibit cell adhesion. The cell proliferation using the MTT assay is depicted in Figure 8. NT-Ag-F showed the highest HGF proliferation at all time intervals. At day 3, NT and NT-Ag showed significantly improved proliferation of HGFs, but this phenomenon was not observed on day 6 and 9. Figure 9 exhibits the ECM-related gene expressions on different surfaces quantified by real-time PCR. Briefly, the HGFs cultured on NT-Ag-F showed advantageous gene expression. The details of the ECM-related gene expressions are summarized in Table IV.

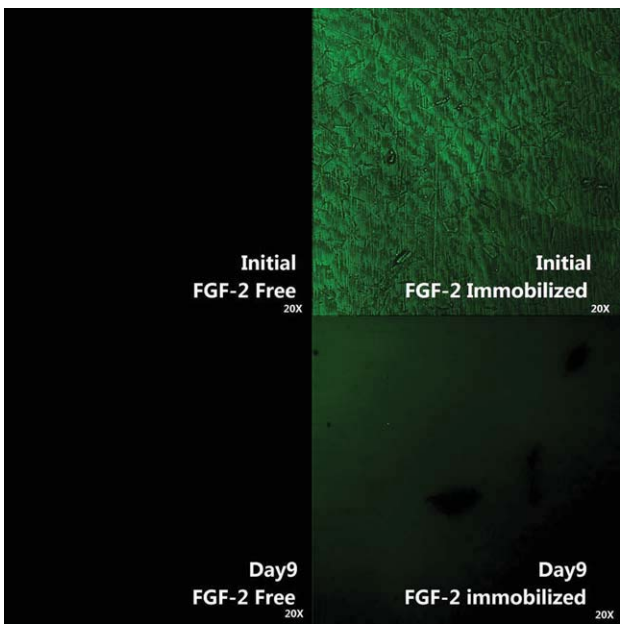

FIGURE 5. Immobilized FGF-2 compared to FGF-2-free samples at day 0 and day 9. [Color figure can be viewed in the online issue, which is available at wileyonlinelibrary.com.]

DISCUSSION

Dental implants, unlike natural teeth, lack protective barriers around the transgingival parts, and thus cannot effectively resist mechanical damage and microbial invasion. Hence, it is crucial to improve the interactions between dental implants and surrounding connective tissue. To prevent the implant from mechanical and bacterial damage, the surface of the Ti implant is modified by anodization followed by immobilizing of Ag nanoparticles and FGF-2 on the nanotubular surface. Although TiO_2 nanotube arrays have drawn much attention for their potential clinical use, the bioactivity is still not well understood. Different types of cells show

TABLE III. Relative Growth Rate (RGR %) According to Cytotoxicity Determination

	24 h	48 h	72 h
Blank	100.00%	100.00%	100.00%
PT	91.39%	87.24%	95.54%
NT	100.86%	110.06%	104.10%
NT-Ag	108.06%	100.77%	95.95%
NT-Ag-F	105.01%	116.33%	97.88%
Cytotoxicity negative control	103.76%	84.44%	92.65%
Cytotoxicity positive control	**0.55%	**0.27%	**0.03%

** ↓($p < 0.01$).

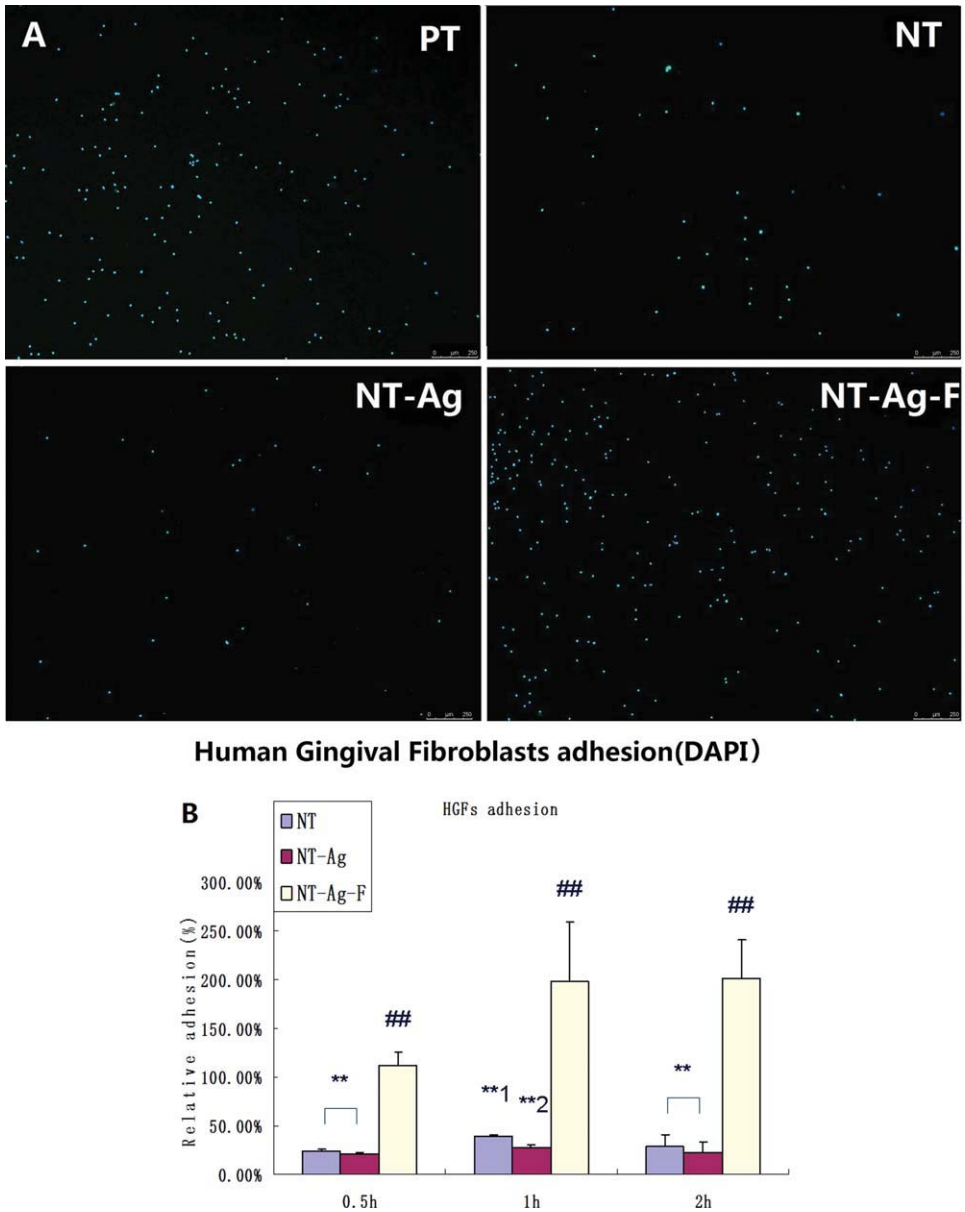

FIGURE 7. HGFs adhesion: (A) HGFs attached to substrates with DAPI stained at 120 min and (B) Relative cell adhesion rate (RCAR) of attached HGFs. Nanotubular surface without FGF-2 inhibits cell adhesion. ## ↑($p < 0.01$), ** ↓($p < 0.01$), difference also exists between **1 and **2 ($p < 0.01$). [Color figure can be viewed in the online issue, which is available at wileyonlinelibrary.com.]

varying reactions on different nanotubular surfaces with various tube sizes.[8–10,12–18] The choice of the sterilization methods can also affect the biocompatibility of TiO_2 surface and UV irradiation has been demonstrated to be one of the sterilization methods capable of improving the bioactivity of TiO_2.[38] In this study, UVA/C irradiation is chosen as our sterilization method. TiO_2 nanotube arrays with size of 100 to 120 nm[18] are applied as a drug-delivery system,[7,8] in which Ag nanoparticles/FGF-2 are used as antibacterial/wound-healing factors.

Immobilization of Ag particles depends on four factors: anodizing voltage, anodizing current, anodizing time, and Ag^+ concentration. According to our previous work, the use of improper conditions can result in the Ag depositing on titania surface with a block form (unpublished data). These four factors must thus be optimized in order to produce a uniform distribution of Ag nanoparticles on the titania surface. Several mechanisms have been postulated to explain the antimicrobial property of Ag nanoparticles. For example, Ag nanoparticles alter the membrane properties of bacteria and degrade lipopolysaccharide molecules causing Ag nanoparticles to accumulate inside the cell membrane, leading to increased membrane permeability.[39] Others suggest that Ag nanoparticles penetrate the bacterial cell, causing DNA damage.[40] It has also been suggested that Ag nanoparticles release a small amount of antimicrobial Ag ions.[41]

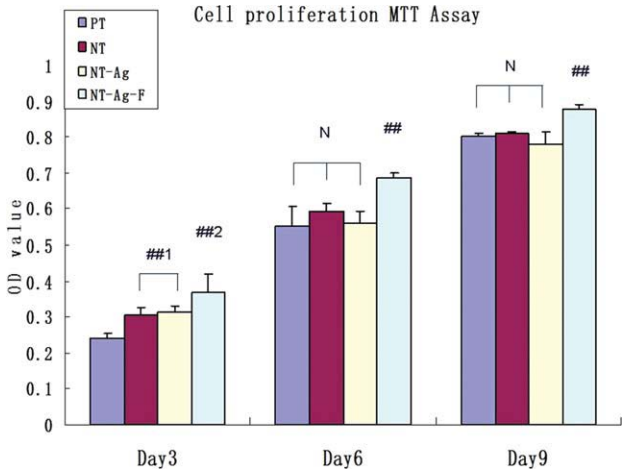

FIGURE 8. Cell proliferation measured by MTT assay. NT-Ag-F had the highest cell proliferation, while NT and NT-Ag show improved cell proliferation in the early stage (Day 3). ## ↑ ($p < 0.01$) and significant difference also exists between ##1 and ##2 ($p < 0.01$). [Color figure can be viewed in the online issue, which is available at wileyonlinelibrary.com.]

Regardless of the mechanism, the antimicrobial properties of Ag nanoparticles have been documented and bacterial drug resistance is very uncommon. It has been reported that Ag^+ ions possess higher cytotoxicity than Ag nanoparticles. Ag^+ ions interact with thiol groups in proteins and inhibit respiratory enzymes, resulting in the production of reactive oxygen species (ROS),[42] which are more toxic to anaerobes than aerobes, preventing DNA replication, and causing DNA damage.[43] It should be noted that the cytotoxicity is dose dependent, and low concentrations of Ag^+ released from the Ag nanoparticles are not cytotoxic.[44] Moreover, noble metals such as silver and gold enable the photocatalytic antimicrobial properties of TiO_2 when excited by visible light,[45–48] and improved antimicrobial activity has been observed without light.[49] In contrast, photocatalytic disinfection by pure TiO_2 can only be activated by UVA ($\lambda =$ 380 nm) irradiation. This non-UVA-dependent antimicrobial property is more useful to the control of peri-implant infection because the oral cavity is not exposed to UVA. FGF-2 is an important regulator of periodontal wound healing and also promotes neovascularization[50] by improving the proliferation potential and ECM secretion of fibroblasts.[29,51] Application of growth factors such as FGF-2 to regenerate periodontal tissues has been described in earlier studies.[52,53] FGF-2 can be immobilized on the O_2 plasma pretreated Ti surface[30] and on hydroxyapatite−Chitosan scaffolds.[54] In this study, a 500 ng/mL FGF-2 solution was used for successive lyophilization without any other specific physical or chemical treatment and the porous TiO_2 nanotubular microstructure might have adhered/absorbed the FGF-2. It is unlikely that FGF-2 reacted with the inert TiO2 nanotubular surface and we infer that the binding form between FGF-2 and NT-Ag surface was one of physical absorption or adhesion rather than other forms of chemical binding. Immunofluorescence evidence demonstrates that FGF-2 is indeed immobilized on the NT-Ag sample surfaces. Even after incubation in PBS for 9 days, FGF-2 was observed on the NT-Ag-F samples. However, it should be noted that the amount of immobilized FGF-2 and the release of immobilized FGF-2 could not be quantified nor controlled accurately.

According to XPS, silver on the TiO_2 nanotubular surface has a zero valence and the FE-SEM images reveal that the Ag nanoparticles with a diameter of about 10 nm are uniformly distributed on the surface, however this phenomenon was not observed in the NT sample. The AFM results indicate that the surface roughness had the following order: PT > NT-Ag-F > NT-Ag > NT. It seems that immobilization of Ag particles/FGF-2 affects the microtopography slightly but increases the roughness of the TiO_2 nanotubular surfaces. Furthermore, immobilization of FGF-2 can also reduce the surface free energy of samples, which may be due to the polarity difference between FGF-2 and TiO_2 nanotubular surface.

Cytotoxicity determination revealed no significant cytotoxicity. The reason may be that the Ag nanoparticle solution only releases negligible amounts of Ag^+ ions[55] and a small concentration of released Ag^+ in the extracts does not cause cytotoxicity.[44] NT and NT-Ag show inhibited cell adhesion but improved cell adhesion is observed from NT-Ag-F, probably due to the surface physicochemical properties and microtopography. The anodized Ti surface possesses a higher surface free energy than polished Ti surface and its porous surface microstructure increases the number of attached osteoblasts.[38] According to AFM, NT, and NT-Ag are not as rough as PT, and HGFs adhere less onto the TiO_2 nanotubular surface. The results are somewhat different from previous data[56] showing that HGF adheres well onto a smooth Ti surface. This difference may be explained by the fact that the TiO_2 nanotubular surface has a small initial cell-substrate contact area with multirings form, which may impair focal adhesion assembly. The impaired focal adhesion assembly results because multirings form cannot support a tight cell-substance integration, and higher surface free energy may also inhibit cell adhesion. The fact that adherence ratio of HGFs to NT-Ag-F is higher than those on the other samples may be caused by immobilization of FGF-2, which may increase cell-substrate contact area and offers various regions to accelerate cell attachment. This positive effect is apparently large enough to reverse the cell adhesion inhibition on the TiO_2 nanotube array. The anodized Ti surface shows improved cell proliferation. The porous-like structure may absorb or store nutrients and nourish cells from beneath. These data indicate that the TiO_2 nanotubular surface shows improved HGF proliferation in early stages, but poor long-term effects. Furthermore, the FGF-2 immobilized titania nanotubular surface (NT-Ag-F) has excellent cytocompatibility as inferred by the highest HGF proliferation at all time points. Our results are in agreement with the behavior of fibroblasts cultured in the FGF-2 added medium.[28] However, not all the immobilized FGF-2 accumulated on the Ti surface can proliferate and lesser proliferation is observed compared to the added medium.[30] This

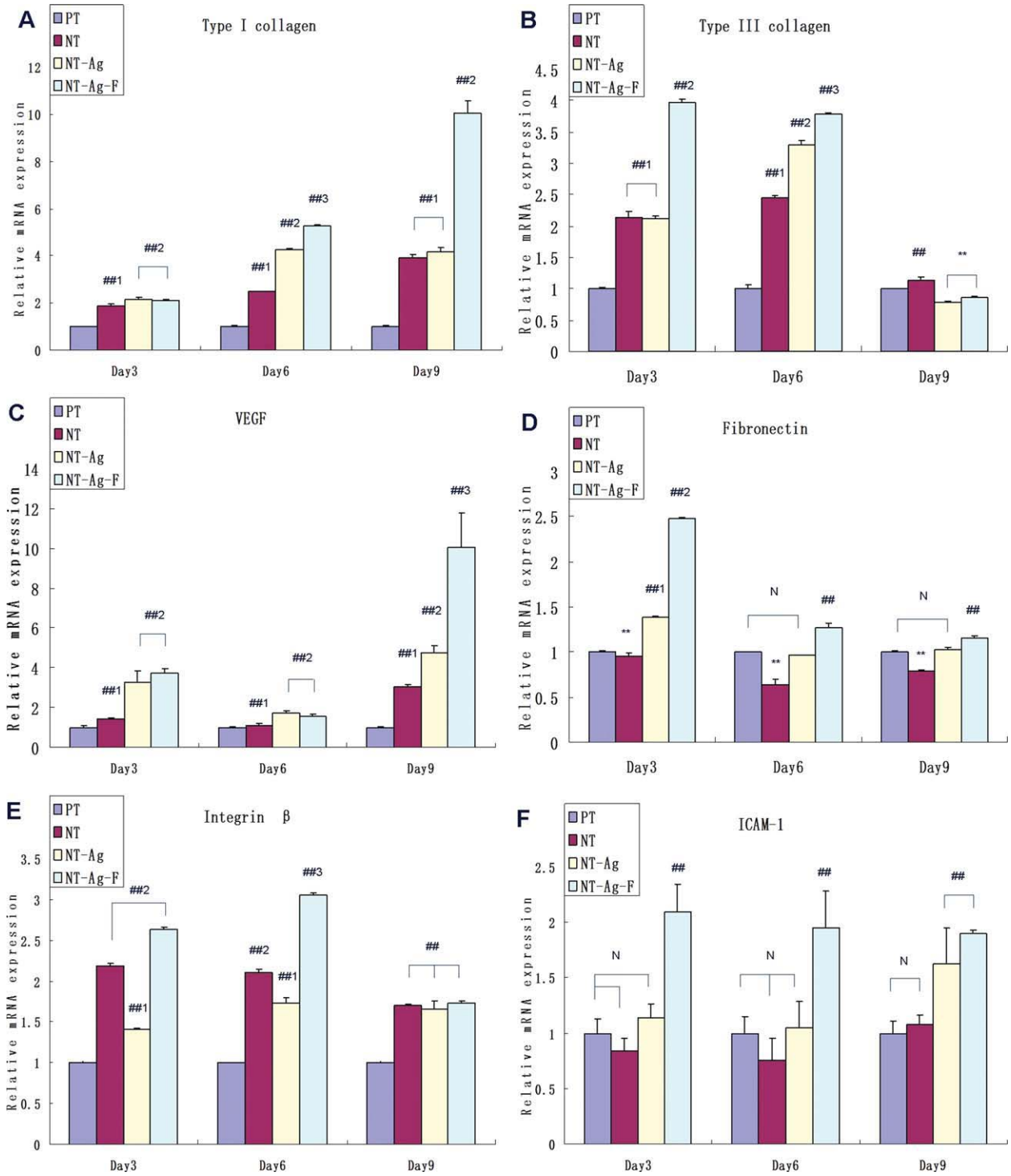

FIGURE 9. ECM-related gene expressions by HGFs cultured on four different Ti surfaces at days 3, 6, and 9: (A) Type I collagen, (B) Type III collagen, (C) VEGF, (D) Fibronectin, (E) Integrin β, and (F) ICAM-1. ## ↑($p < 0.01$), ** ↓($p < 0.01$). [Color figure can be viewed in the online issue, which is available at wileyonlinelibrary.com.]

may be due to the non-availability of some functional groups on the FGF-2 immobilized on the TiO_2—steric hindrance.

Type I/III collagen, the main component in gingival tissues, are associated with wound healing. Bundles of well-developed collagen fibers and elongated fibroblasts are observed surrounding the cell layer and they are parallel to the long axis of the implant. These fibers are believed to provide effective sealing of the peri-implant tissues from the oral environment.[57] It has been reported that at days 14

TABLE IV. Summary of ECM-Related Gene Expressions

	NT			NT-Ag			NT-Ag-F		
	D3	D6	D9	D3	D6	D9	D3	D6	D9
Type I collagen	+	+	+	+2	+2	+	+2	+3	+2
Type III collagen	+	+	+	+	+2	–	+2	+3	–
VEGF	+	+	+	+2	+	+	+2	+2	+3
Fibronectin	–	–	–	+	/	/	+2	+	+
Integrin β	+2	+2	+	+	+	+	+2	+3	+
ICAM-1	/	/	/	/	/	+	+	+	+
Laminin	+	+	+	+2	+2	+2	+2	+3	+3

Details of gene expressions at days 3, 6, and 9. "+" = up-regulate; "–" = down-regulate; "/" = no significant difference compared to PT; +3 > +2 > +; difference exists between +3, +2, +, /, and –.

and 28, collagen I and collagen III mRNA expressions are enhanced significantly after addition of 3 ng/mL FGF-2.[58] Although the appropriate collagen synthesis has a positive effect on tissue healing of the peri-implant soft tissues, over-synthesis of type III collagen may induce oral sub-mucous fibrosis.[59] In this work, the type I collagen expressions of NT, NT-Ag, and NT-Ag-F are elevated at all time periods studied, corresponding to that of a low-dose FGF-2 reported previously.[58] Both FGF-2 and TiO_2 nanotubular surfaces can enhance type I collagen expression of HGFs and Ag nanoparticles do not impede this function. There are some differences in the type III collagen expression on days 3 and 6, and the type III collagen expressions on NT, NT-Ag, and NT-Ag-F are up-regulated compared to NT-Ag-F. However, at day 9, only type III collagen expression on NT is up-regulated, whereas suppressive effects are observed from NT-Ag and NT-Ag-F. The TiO_2 nanotubular surface can enhance type III collagen expression in the long run, but Ag nanoparticles may prevent over-expression of type III collagen, thereby hampering peri-implant tissue fibrosis. VEGF, which is a macromolecule that can enhance blood vessel growth and permeability,[60] is a powerful mitogen for endothelial cells fulfilling an important role in angiogenesis.[61] VEGF mRNAs are up-regulated when bone marrow stromal cells (MSCs) are cultured with FGF-2 at concentrations of 1 to 25 ng/mL.[62] Cross-communication between FGFs, VEGF, and inflammatory cytokines/chemokines may play a role in the modulation of blood vessel growth.[26] Hence, immobilization of FGF-2 on the titania surface may promote vascularization and eventual regeneration of gingival tissues around the dental implants. In this study, VEGF expression was elevated in NT, NT-Ag, and NT-Ag-F. NT-Ag and NT-Ag-F had higher gene expression than NT, indicating that Ag nanoparticles can also up-regulate the VEGF expression. There was no significant difference between NT-Ag and NT-Ag-F on days 3 and 6, but on day 9, NT-Ag-F shows obviously higher gene expression of VEGF than NT-Ag. The results suggest vascularization promoted by FGF-2 is not activated in the early stage in contrast to Ag nanoparticles. In the early stage, excess vascularization may lead to tissue inflammation or edema delaying tissue healing and this delayed angiogenesis function is consistent with the normal wound healing processes. Fibronectin, a major component of serum and the periodontal tissues critical to wound healing,[63] plays an important role in the early wound healing events such as cell migration and adhesion.[64] Fibronectin can also increase the vasopermeability[65] and enhances polymorphonuclear neutrophil (PMN) migration. The response is mediated by the alpha5beta1 FN receptor.[66] Our results suggest that the TiO_2 nanotubular surface may suppress fibronectin expression but Ag nanoparticles can offset this negative function. Furthermore, FGF-2 can up-regulate Fibronectin expression yielding the same result as reported previously.[58] This promoting effect can improve cell migration and adhesion, which contribute to gingival tissue healing around the implants, increase the recruit of PMN, and control infection around the implants. But the immunologically mediated damage can not be ignored. Integrins are specialized adhesive molecules in cell-to-cell and cell-to-substrate adhesion.[67] Integrin β is important in cellular binding on coated or textured titanium implants.[68] It has been found from the periodontium of rats and humans and is known to play an important role in the attachment of cells in these tissues.[69–71] eTotal beta1-integrin expression levels are dose-dependent and increased by FGF-2.[72] In this study, NT, NT-Ag, and NT-Ag-F up-regulate the Integrin β expression at all time and NT-Ag-F shows the highest gene expression among them. At days 3 and 6, NT exhibits higher Integrin β expression than NT-Ag. This trend vanishes at day 9 when no significant difference was observed among NT, NT-Ag, and NT-Ag-F. The results reveal that Ag nanoparticles/FGF-2 may suppress/up-regulate gene expression of Integrin β in the early stage, and the gene inhibition by the Ag nanoparticles may cause gene-toxicity. Over the longer term ($\geq$ 9 days), the TiO_2 nanotubular surface is probably the main factor regulating the gene expression of Integrin β. ICAM-1 is a widely expressed adhesion molecule and belongs to the I_g super family. It may play an important physiological role in efficiently routing PMNs to the gingival sulcus. This process contributes to the maintenance of local host-parasite equilibrium and limitation of PMN-associated tissue damage.[73] ICAM-1 is also associated with endothelial cells both in healthy and inflamed tissues and may be critical in processes directing leukocyte migration towards the gingival sulcus. Besides its immunological functions, ICAM-1 mediates cell-cell adhesion.[74–76] The expression of the endothelial cell

adhesion molecules (CAMs) for leukocytes, P-selectin, E-selectin, and ICAM-1, is significantly up-regulated on the inflamed tissues by FGF-2.[77] Here, our results reveal that the TiO_2 nanotubular surface does not regulate the ICAM-1 expression but NT-Ag-F significantly up-regulates the ICAM-1 expression of HGFs at all three time intervals studied. The Ag nanoparticles may also contribute to the up-regulation of ICAM-1 expression but there is no obvious difference between NT-Ag and NT-Ag-F at day 9. This up-regulation not only may increase intercellular adhesion, but also recruit PMN to exert anti-infective functions in gingival sulcus. Ag/FGF-2 immobilization has a potential to routinely control the subgingival plaque after and may possibly improve the microecological environment around the dental implant.

CONCLUSION

Ag nanoparticles attached to the modified Ti surface show extremely low cytotoxicity and the immobilized FGF-2 is potent enough to enhance HGF cell attachment, proliferation, and ECM-related gene expression. Unexpected bioactivity is observed from the Ag nanoparticles pertaining to ECM-related gene expression, but more work is needed in order to fully understand this mechanism. The TiO_2 nanotubular surface with immobilized compound Ag/FGF-2 has excellent cytocompatibility compared to pure Ti and this modified Ti surface may have potential use in dental implant abutment.

REFERENCES

1. Adell R, Eriksson B, Lekholm U, Brånemark PI, Jemt T. Long-term follow-up study of osseointegrated implants in the treatment of totally edentulous jaws. Int J Oral Maxillofac Implants 1990;5: 347–359.
2. Arvidson K, Bystedt H, Frykholm A, von Konow L, Lothigius E. Five-year prospective follow-up report of the Astra Tech Dental Implant System in the treatment of edentulous mandibles. Clin Oral Implants Res 1998;9:225–234.
3. Olsson M, Gunne J, Astrand P, Borg K. Bridges supported by free-standing implants versus bridges supported by tooth and implant. A five-year prospective study. Clin Oral Implants Res 1995;6:114–121.
4. Chehroudi B, Gould TR, Brunette DM. The role of connective tissue in inhibiting epithelial downgrowth on titanium-coated percutaneous implants. J Biomed Mater Res 1992;26:493–515.
5. Brunette DM. Effects of surface topography of implant materialson on cell behavior in vitro and in vivo in Nanofabrication and Biosystems. In Hoch HC, Jelinski LW, Craighead HG, eds. Cambridge University Press, Cambridge, UK. 1996:335–355.
6. Gong D, Grimes CA, Varghese OK, Chen Z, Hu W, Dickey EC. Titanium oxide nanotube arrays prepared by anodic oxidation. J Mater Res 2001;12:3331–3334.
7. Eaninwene G,II, Yao C, Webster TJ. Enhanced osteoblast adhesion to drug coated anodized nanotubular titanium surfaces. Int J Nanomedicine 2008;3:257–264.
8. Balasundaram G, Yao C, Webster TJ. TiO2 nanotubes functionalized with regions of bone morphogenetic protein-2 increases osteoblast adhesion. J Biomed Mater Res A 2008;84:447–453.
9. Park J, Bauer S, von der Mark K, Schmuki P. Nanosize and vitality: TiO2 nanotube diameter directs cell fate. Nano Lett 2007;7: 1686–1691.
10. Brammer KS, Oh S, Cobb CJ, Bjursten LM, Heyd HV, Jin S. Improved bone-forming functionality on diameter-controlled TiO2 nanotube surface. Acta Biomater 2009;5:3215–3223.
11. von Wilmowsky C, Bauer S, Lutz R, Meisel M, Neukam FW, Toyoshima T, Schmuki P, Nkenke E, Schlegel KA. In vivo evaluation of anodic TiO2 nanotubes: An experimental study in the pig. J Biomed Mater Res B 2009;89:165–171.
12. Oh S, Daraio C, Chen LH, Pisanic TR, Fiñones RR, Jin S. Significantly accelerated osteoblast cell growth on aligned TiO2 nanotubes. J Biomed Mater Res A 2006;78:97–103.
13. Popat KC, Eltgroth M, Latempa TJ, Grimes CA, Desai TA. Decreased Staphylococcus epidermis adhesion and increased osteoblast functionality on antibiotic-loaded titania nanotubes. Biomaterials 2007;28:4880–4888.
14. Das K, Bose S, Bandyopadhyay A. TiO2 nanotubes on Ti: Influence of nanoscale morphology on bone cell-materials interaction. J Biomed Mater Res A 2009;90:225–237.
15. Popat KC, Leoni L, Grimes CA, Desai TA. Influence of engineered titania nanotubular surfaces on bone cells. Biomaterials 2007;28: 3188–3197.
16. Oh S, Brammer KS, Li YS, Teng D, Engler AJ, Chien S, Jin S. Stem cell fate dictated solely by altered nanotube dimension. Proc Natl Acad Sci U S A. 2009;106:2130–2135.
17. von der Mark K, Bauer S, Park J, Schmuki P. Another look at "Stem cell fate dictated solely by altered nanotube dimension". Proc Natl Acad Sci U S A. 2009;106:E60; author reply E61.
18. Demetrescu I, Pirvu C, Mitran V. Effect of nano-topographical features of Ti/TiO2 electrode surface on cell response and electrochemical stability in artificial saliva. Bioelectrochemistry 2010;79: 122–129.
19. Das K, Bose S, Bandyopadhyay A, Karandikar B, Gibbins BL. Surface coatings for improvement of bone cell materials and antimicrobial activities of Ti implants. J Biomed Mater Res B Appl Biomater 2008;87:455–460.
20. Kawashita M, Tsuneyama S, Miyaji F, Kokubo T, Kozuka H, Yamamoto K. Antibacterial silver-containing silica glass prepared by sol-gel method. Biomaterials 2000;21:393–398.
21. Uchida M. Antibacterial zeolite and its application. Chem Ind 1995;46:48–54.
22. Xu XH, Brownlow WJ, Kyriacou SV, Wan Q, Viola JJ. Real-time probing of membrane transport in living microbial cells using single nanoparticle optics and living cell imaging. Biochemistry 2004;43:10400–10413.
23. Gogoi SK, Gopinath P, Paul A, Ramesh A, Ghosh SS, Chattopadhyay A. Green fluorescent protein-expressing Escherichia coli as a model system for investigating the antimicrobial activities of silver nanoparticles. Langmuir 2006;22:9322–9328.
24. Ornitz DM, Itoh N. Fibroblast growth factors. Genome Biol 2001;2: REVIEWS3005.
25. Kanda S, Lerner EC, Tsuda S, Shono T, Kanetake H, Smithgall TE. The nonreceptor protein-tyrosine kinase c-Fes is involved in fibroblast growth factor-2-induced chemotaxis of murine brain capillary endothelial cells. J Biol Chem 2000;275: 10105–10111.
26. Presta M, Dell'Era P, Mitola S, Moroni E, Ronca R, Rusnati M. Fibroblast growth factor/fibroblast growth factor receptor system in angiogenesis. Cytokine Growth Factor Rev 2005;16:159–178.
27. Gerritsen ME, Soriano R, Yang S, Zlot C, Ingle G, Toy K, Williams PM. Branching out: A molecular fingerprint of endothelial differentiation into tube-like structures generated by Affymetrix oligonucleotide arrays. Microcirculation 2003;10:63–81.
28. Palmon A, Roos H, Edel J, Zax B, Savion N, Grosskop A, Pitaru S. Inverse dose- and time-dependent effect of basic fibroblast growth factor on the gene expression of collagen type I and matrix metalloproteinase-1 by periodontal ligament cells in culture. J Periodontol 2000;71:974–980.
29. Takayama S, Murakami S, Miki Y, Ikezawa K, Tasaka S, Terashima A, Asano T, Okada H. Effects of basic fibroblast growth factor on human periodontal ligament cells. J Periodontal Res 1997;32: 667–675.
30. Kokubu E, Yoshinari M, Matsuzaka K, Inoue T. [title] Behavior of rat periodontal ligament cells on fibroblast growth factor-2-immobilized titanium surfaces treated by plasma modification. J Biomed Mater Res A 2009;91:69–75.
31. Mustafa K, Silva LB, Hultenby K, Wennerberg A, Arvidson K. Attachment and proliferation of human oral fibroblasts to

titanium surfaces blasted with TiO2 particles. A scanning electron microscopic and histomorphometric analysis. Clin Oral Implants Res 1998;9:195–207.
32. Yoshinari M, Matsuzaka K, Inoue T, Oda Y, Shimono M. Effects of multigrooved surfaces on fibroblast behavior. J Biomed Mater Res A 2003;65:359–368.
33. Kim SY, Oh N, Lee MH, Kim SE, Leesungbok R, Lee SW. Surface microgrooves and acid etching on titanium substrata alter various cell behaviors of cultured human gingival fibroblasts. Clin Oral Implants Res 2009;20:262–272.
34. Owens DK, Wendt RG. J Appl Polym sci 1969;13:1741.
35. International Organization for Standardization. Biological evaluation of medical devices-ISO 10993–5, Part 5: Tests for in vitro cytotoxicity. Geneva, Switzerland; 2009(E).
36. Coecke S, Balls M, Bowe G, Davis J, Gstraunthaler G, Hartung T, Hay R, Merten OW, Price A, Schechtman L, Stacey G, Stokes W. Second ECVAM Task Force on Good Cell Culture Practice. Guidance on good cell culture practice: A report of the second ECVAM task force on good cell culture practice. Altern Lab Anim 2005;33:261–287.
37. Wagner CD, Riggs wM, Davis LE, Moulder JF. Handbook of X-ray Photoelectron Spectroscopy: A reference book of standard data for use in x-ray photoelectron spectroscopy. Minnesota: Perkin Elmer Corporation; 1979. p 112.
38. Zhao L, Mei S, Wang W, Chu PK, Wu Z, Zhang Y. The role of sterilization in the cyto-compatibility of titania nanotubes. Biomaterials 2010;31:2055–2063.
39. Sondi I, Salopek-Sondi B. Silver nanoparticles as antimicrobial agent: A case study on E. coli as a model for gram-negative bacteria. J Colloid Interface Sci 2004;275:177–182.
40. AshaRani PV, Low Kah Mun G, Hande MP, Valiyaveettil S. Cytotoxicity and genotoxicity of silver nanoparticles in human cells. ACS Nano 2009;3:279–290.
41. Morones JR, Elechiguerra JL, Camacho A, Holt K, Kouri JB, Ramirez JT, Yacaman MJ. The bactericidal effect of silver nanoparticles. Nanotechnology 2005;16:2346–2353.
42. Matsumura Y, Yoshikata K, Kunisaki S, Tsuchido T. Mode of bactericidal action of silver zeolite and its comparison with that of silver nitrate. Appl Environ Microbiol 2003;69:4278–4281.
43. Feng QL, Wu J, Chen GQ, Cui FZ, Kim TN, Kim JO. A mechanistic study of the antibacterial effect of silver ions on Escherichia coli and Staphylococcus aureus. J Biomed Mater Res 2000;52:662–668.
44. Williams RL, Doherty PJ, Vince DG, Grasho GJ, Williams DF. The biocompatibility of silver. Crit Rev Biocomp 1989;5:221–243.
45. Paramasivam I, Macak JM, Schmuki P. Photocatalytic activity of TiO2 nanotube layers loaded with Ag and Au nanoparticles. Electrochem Commun 2009;10:71–75.
46. Seery MK, George R, Floris P, Suresh CP. Silver doped titanium dioxide nanomaterials for enhanced visible light photocatalysis. J Photochem Photobiol A 2007;(2–3):258–263
47. Page K, Palgrave RG, Parkin IP, Wilson M, Savin SLP, Chadwick AV. 2007. Titania and silver-titania composite films on glass-potent antimicrobial coatings. J Mater Chem 2007;17:95–104.
48. Reddy MP, Venugopal A, Subrahmanyam M. Hydroxyapatite-supported Ag-TiO2 as Escherichia coli disinfection photocatalyst. Water Res 2007;41:379–386.
49. Akhavan O. Lasting antibacterial activities of Ag-TiO2/Ag/a-TiO2 nanocomposite thin film photocatalysts under solar light irradiation. J Colloid Interface Sci 2009;336:117–124.
50. Shimono M, Ishikawa T, Ishikawa H, Matsuzaki H, Hashimoto S, Muramatsu T, Shima K, Matsuzaka K, Inoue T. Regulatory mechanisms of periodontal regeneration. Microsc Res Tech 2003;60: 491–502.
51. Pitaru S, Kotev-Emeth S, Noff D, Kaffuler S, Savion N. Effect of basic fibroblast growth factor on the growth and differentiation of adult stromal bone marrow cells: Enhanced development of mineralized bone-like tissue in culture. J Bone Miner Res 1993;8: 919–929.
52. Murakami S, Takayama S, Ikezawa K, Shimabukuro Y, Kitamura M, Nozaki T, Terashima A, Asano T, Okada H. Regeneration of periodontal tissues by basic fibroblast growth factor. J Periodontal Res 1999;34:425–430.
53. Nakahara T, Nakamura T, Kobayashi E, Inoue M, Shigeno K, Tabata Y, Eto K, Shimizu Y. Novel approach to regeneration of periodontal tissues based on in situ tissue engineering: Effects of controlled release of basic fibroblast growth factor from a sandwich membrane. Tissue Eng 2003;9:153–162.
54. Akman AC, Tiğli RS, Gümüşderelioğlu M, Nohutcu RM. bFGF-loaded HA-chitosan: A promising scaffold for periodontal tissue engineering. J Biomed Mater Res A 2010;92:953–962.
55. Li PW, Kuo TH, Chang JH, Yeh JM, Chan WH. Induction of cytotoxicity and apoptosis in mouse blastocysts by silver nanoparticles. Toxicol Lett 2010;197:82–87.
56. Mustafa K, Odqn A, Wennerberg A, Hultenby K, Arvidson K. The influence of surface topography of ceramic abutments on the attachment and proliferation of human oral fibroblasts. Biomaterials 2005;26:373–381.
57. Shioya K, Sawada T, Miake Y, Inoue S, Yanagisawa T. Ultrastructural study of tissues surrounding replanted teeth and dental implants. Clin Oral Implants Res 2009;20:299–305.
58. Hankemeier S, Keus M, Zeichen J, Jagodzinski M, Barkhausen T, Bosch U, Krettek C, Van Griensven M. Modulation of proliferation and differentiation of human bone marrow stromal cells by fibroblast growth factor 2: Potential implications for tissue engineering of tendons and ligaments. Tissue Eng 2005;11:41–49.
59. Kuo MY, Chen HM, Hahn LJ, Hsieh CC, Chiang CP. Collagen biosynthesis in human oral submucous fibrosis fibroblast cultures. J Dent Res 1995;74:1783–1788.
60. Johnson RB, Serio FG, Dai X. Vascular endothelial growth factors and progression of periodontal diseases. J Periodontol 1999;70: 848–852.
61. Connolly DT. Vascular permeability factor: A unique regulator of blood vessel function. J Cell Biochem 1991;47:219–223.
62. Farhadi J, Jaquiery C, Barbero A, Jakob M, Schaeren S, Pierer G, Heberer M, Martin I. Differentiation-dependent up-regulation of BMP-2, TGF-beta1, and VEGF expression by FGF-2 in human bone marrow stromal cells. Plast Reconstr Surg 2005;116: 1379–1386.
63. Steffensen B, Häkkinen L, Larjava H. Proteolytic events of wound-healing–coordinated interactions among matrix metalloproteinases (MMPs), integrins, and extracellular matrix molecules. Crit Rev Oral Biol Med 2001;12:373–398.
64. Jones RA, Nicholas B, Mian S, Davies PJA, Griffin M. Reduced expression of tissue transglutaminase in a human endothelial cell line leads to changes in cell spreading, cell adhesion and reduced polymerization of fibronectin. J Cell Sci 1997;110: 2461–2472.
65. Nakagawa T, Yamane H, Shigeta T, Takashima T, Nakai Y. Interaction between fibronectin and eosinophils in the growth of nasal polyps. Laryngoscope 1999;109:557–561.
66. Everitt EA, Malik AB, Hendey B. Fibronectin enhances the migration rate of human neutrophils in vitro. J Leukoc Biol 1996;60: 199–206.
67. Diamond MS, Springer TA. The dynamic regulation of integrin adhesiveness. Curr Biol 1994;4:506–517.
68. Kramer PR, Janikkeith A, Cai Z, Ma S, Watanabe I. Integrin mediated attachment of periodontal ligament to titanium surfaces. Dent Mater 2009;25:877–883.
69. Bolcato-Bellemin AL, Elkaim R, Abehsera A, Fausser JL, Haikel Y, Tenenbaum H. Expression of mRNAs encoding for alpha and beta integrin subunits. MMPs, and TIMPs in stretched human periodontal ligament and gingival fibroblasts. J Dent Res 2000;79: 1712–1716.
70. Matias MA, Li H, Young WG, Bartold PM. Immunohistochemical localisation of extracellular matrix proteins in the periodontium during cementogenesis in the rat molar. Arch Oral Biol 2003;48: 709–716.
71. Ivanovski S, Komaki M, Bartold PM, Narayanan AS. Periodontal-derived cells attach to cementum attachment protein via alpha 5 beta 1 integrin. J Periodontal Res 1999;34:154–159.
72. Yanagisawa M, Yagi H, Nakatani Y, Yu RK. Involvement of beta1-integrin up-regulation in basic fibroblast growth factor- and epidermal growth factor-induced proliferation of mouse neuroepithelial cells. J Biol Chem 2010;285:18443–18451.

73. Tonetti MS, Imboden MA, Lang NP. Neutrophil migration into the gingival sulcus is associated with transepithelial gradients of interleukin-8 and ICAM-1. J Periodontol 1998;69:1139–1147.
74. Crawford JM, Hopp B. Junctional epithelium expresses the intercellular adhesion molecule ICAM-1. J Periodontal Res. 1990;25: 254–256.
75. Norris P, Poston RN, Thomas DS, Thornhill M, Hawk J, Haskard DO. The expression of endothelial leukocyte adhesion molecule-1 (ELAM-1), intercellular adhesion molecule-1 (ICAM-1) and vascular cell adhesion molecule-1 (VCAM-1) in experimental cutaneous inflammation: A comparison of ultraviolet Berythema and delayed hypersensitivity. J Invest Dermatol 1991;96: 763–770.
76. Moughal NA, Adonogianaki E, Thornhill MH, Kinane DF. Endothelial cell leukocyte adhesion molecule-1 (ELAM-1) and intercellular adhesion molecule-1 (ICAM-1) expression in gingival tissue during health and experimentally-induced gingivitis. J Periodontal Res 1992;27:623–630.
77. Zittermann SI, Issekutz AC. Basic fibroblast growth factor (bFGF. FGF-2) potentiates leukocyte recruitment to inflammation by enhancing endothelial adhesion molecule expression. Am J Pathol 2006;168:835–846.